

Nucleation and Growth Process of Sodalite and Cancrinite from Kaolinite-rich Clay under Low-temperature Hydrothermal Conditions

Carlos Alberto Ríos Reyes^{a*}, Craig Williams^b, Oscar Mauricio Castellanos Alarcón^c

^aEscuela de Geología, Universidad Industrial de Santander, Carrera 27 Calle 9, Ciudad Universitaria, Bucaramanga, Colombia

^bSchool of Applied Sciences, University of Wolverhampton, Wulfruna Street, Wolverhampton WV1 1SB, England

^cPrograma de Geología, Universidad de Pamplona, Ciudad Universitaria, Pamplona, Colombia

Received: October 28, 2011; Revised: August 24, 2012

The synthesis of low-silica zeotypes by hydrothermal transformation of kaolinite-rich clay and the nucleation and growth processes of sodalite and cancrinite in the system $\text{Na}_2\text{O}-\text{Al}_2\text{O}_3-\text{SiO}_2-\text{H}_2\text{O}$ at 100 °C were investigated. The synthesis products were characterized by X-ray powder diffraction (XRPD), scanning electron microscopy (SEM), Fourier transform infrared spectroscopy (FT-IR), ²⁹Si and ²⁷Al Magic Angle Spinning Nuclear Magnetic Resonance (MAS-NMR) and thermogravimetric analysis (TGA). Our data show that the sequence of the transformation of phases is: Poorly crystalline aluminosilicate → zeolite LTA → sodalite → sodalite + cancrinite → cancrinite. Synthesized materials appeared stable thermodynamically under the experimental conditions, with zeolite LTA (a metastable phase) occurring as a minor phase, compared with the presence of sodalite and cancrinite.

Keywords: synthesis, low-silica, hydrothermal, kaolinite, transformation

1. Introduction

The Bayer process is the principal industrial means of refining bauxite to produce alumina (Al_2O_3), which must be purified before it can be refined to aluminium metal. During alumina production, bauxite is digested by washing with a hot solution of sodium hydroxide (NaOH) at elevated temperatures¹. SiO_2 , an impurity in the bauxite in the form of kaolinite and quartz, can also be digested. After digestion, the dissolved SiO_2 subsequently reacts with the ionic species in the sodium aluminate solution to form a “desilication product” (commonly known as DSP) which primarily consists sodium aluminosilicates, such as sodalite (SOD) and cancrinite (CAN)¹⁻⁴. Both SOD and CAN are of the common chemical formula $\text{Na}_6[\text{Al}_6\text{Si}_6\text{O}_{24}]\cdot 2\text{NaX}\cdot 6\text{H}_2\text{O}$, where X can be OH^- , Cl^- , NO_3^- , $1/2\text{CO}_3^{2-}$, or $1/2\text{SO}_4^{2-}$.

However, their structural frameworks are different (Figure 1). SOD has a cubic framework that contains only β -cages made up of eight 6-membered rings of alternating AlO_4 and SiO_4 tetrahedra and six 4-membered rings; the free dimension of the inscribed sphere of the β -cage is 6.6 Å and access to the cage through the 6-membered ring window (channel) is ~2.2 Å^[3]. CAN has a hexagonal framework that contains small ϵ -cages consisting of five 6-membered rings and six 4-membered rings, which give rise to large continuous channels consisting of 12-membered rings with a free dimension of ~6.2 Å^[5]. In general, these aluminosilicates are characterized by a three-dimensional framework, which contain cages and channels in their negatively charged frameworks because of the substitution of Si^{4+} ions by Al^{3+} ions⁶. Both the β - and ϵ - cages need

positively charged species to neutralise them³. Cations can enter these porous materials to balance the charge of their structural frameworks⁶. Structural data of these zeolite frameworks are published by the ‘Structure Commission of the International Zeolite Association’ (IZA)⁷.

The low-temperature hydrothermal conversion of kaolinite and metakaolinite to low silica zeolites (LSZs) is a very well known process, with zeolite LTA as the most common synthesis product⁸, which is a metastable phase during the formation of SOD and CAN. The synthesis of zeolites from kaolinite has been extensively investigated^{5,9}. However, the improvement of the kaolinite properties by chemical methods is difficult due to its low reactivity; this clay mineral is not significantly affected by acid or alkaline treatments, even under strong conditions¹⁰. Therefore, kaolinite is usually used after calcination at temperatures between 550-950 °C¹¹ to obtain a more reactive phase (metakaolinite) under chemical treatments. Several authors have reported the synthesis of metakaolinite-based zeolitic materials, including the zeolite LTA^{8,12-15}. The mechanisms and kinetics of SOD and CAN formation have been investigated by several authors^{1-3,16}. According to Barnes et al.², the phase transformation from SOD to CAN was a solution-mediated process, which involved a four-stage mechanism. However, there are many inconsistencies in the published sodium aluminosilicate equilibrium solubility data particularly for the SOD and CAN phases¹⁷. On the other hand, whether or not the crystalline phase underwent any transformation changes (e.g. SOD to CAN) was either not determined or not taken into account¹⁸.

*e-mail: carios@uis.edu.co

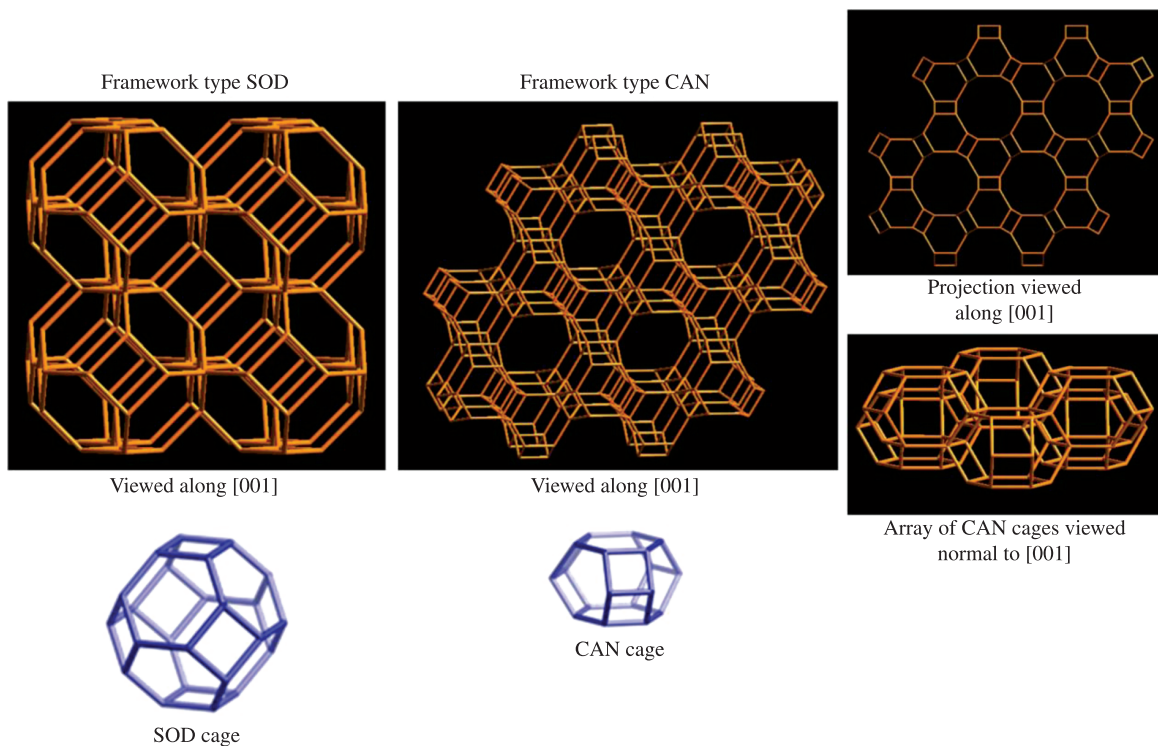


Figure 1. Framework structures of SOD and CAN, showing their characteristic cages and channels, adopted and modified from the Database of Zeolite Structures⁷.

In this work, we investigate not only the low-temperature hydrothermal transformation of kaolinite and metakaolinite into SOD and CAN-type structures but also the phase transformation from SOD to CAN. On the other hand, this research is also useful in order to understand the common natural process of low to medium temperature alteration of feldspatoids in alkaline volcanic and subvolcanic rocks.

2. Experimental

2.1. Material

The raw material used in this study was a kaolinite-rich clay (distributed under the name Supreme Powder and supplied by English China Clay International). Metakaolinite was obtained by thermal treatment at 600 °C of the kaolinite-rich clay. Both kaolinite and metakaolinite were used as starting materials for the synthesis of zeotypes. Other reagents used in the activation of the raw materials were: sodium hydroxide, NaOH, as pellets (99.99%, Aldrich Chemical Company, Inc.) and distilled water using standard purification methods.

2.2. Synthesis of SOD- and CAN-type structures

Zeotype synthesis was carried out under hydrothermal conditions in alkaline medium using kaolinite and metakaolinite as silica and alumina sources. A calculated amount of alkali hydroxide pellets was added to distilled water in reaction plastic beakers (150-250 mL) to prepare 1.33 M and 3.99 M NaOH solutions; the starting materials

were then mixed with the alkaline solutions to produce a reaction gel with a specific molar composition. The progressive addition of reagents was carried out under stirring conditions until they dissolved to homogenize the reaction gels. Crystallization was carried out by hydrothermal synthesis under static conditions in PTFE vessels of 65 mL at 100 °C for several reaction times. Once the activation time was reached, the reactors were removed from the oven and quenched in cold water to stop the reaction. After hydrothermal treatment, the reaction mixtures were filtered and washed with distilled water to remove excess alkali until the pH of the filtrate became neutral. Then, the samples were oven dried at 80 °C overnight. The hydrogel pH was measured before and after hydrothermal treatment. The dried samples were weighted and kept in plastic bags for characterization. Table 1 presents the experimental conditions used for zeolite synthesis.

2.3. Characterization of the starting materials and as-synthesized zeotypes

X-ray diffraction (XRD) patterns of the starting materials and as-synthesized zeotypes were recorded using a Philips PW1710 diffractometer operating in Bragg-Brentano geometry with Cu-K α radiation (40 kV and 40 mA) and secondary monochromation. Data collection was carried out in the 2 θ range 3-50°, with a step size of 0.02°, a divergent slit of 1.0°, and a dwell time of 2 seconds. Phase identification was performed by searching the ICDD powder diffraction file database, with the help of JCPDS files for inorganic compounds. The morphology of the solid phases were

examined in a ZEISS EVO50 scanning electron microscopy (SEM) under the following analytical conditions: 1 probe 1 nA, EHT = 20.00 kV, beam current 100 μ A, Signal A = SE1, WD = 8.0 mm. Specimens were prepared by spraying dried raw material or zeolite powder onto aluminium stubs using double-sided adhesive carbon discs and sputter coated with gold to reduce static charging and then observing under SEM conditions. For EDX analysis the samples were prepared in a similar way to SEM. However, to avoid errors in the aluminium content, a carbon sample holder was used instead of aluminium stud and gold was not coated on the samples. Fourier transform infrared (FT-IR) spectroscopy was performed using a Mattson Genesis II FT-IR spectrometer in the 4000-400 cm^{-1} region. However, only the 1200-400 cm^{-1} region was investigated, taking into account that it is where the spectra showed remarkable changes. Solid-state ^{29}Si and ^{27}Al Magic Angle Spinning Nuclear Magnetic Resonance (MAS NMR) spectra were recorded on a Varian UnityInova spectrometer under the following analytical conditions: MAS probe 7.5-4.0 mm; frequency 59.6-78.1 MHz; spectral width 29996-100000 Hz; acquisition time 30-10 ms; recycle time 120-0.5 seconds; number of repetitions 15-2200; spinning rate 5040-14000 Hz; pulse angle $\pi/2$ - $\pi/10$. The chemical

shifts were referenced to tetramethylsilane (TMS) for ^{29}Si and 1 M AlCl_3 aqueous solution for ^{27}Al . Thermogravimetric analyses (TGA) were performed on a Mettler Toledo TG 50 thermobalance between 25-700 $^{\circ}\text{C}$ at a heating rate of 20 $^{\circ}\text{C}/\text{min}$ under flowing air (200 cm^3/min). The ground sample was directly filled into the crucible for testing. The amount was normally \sim 15-20 mg to minimize background noise.

3. Results and Discussion

3.1. Starting materials

The XRD patterns of the starting materials are presented in Figure 2. Kaolinite (Figure 2a) in the sample is identified by its characteristic XRD peaks at 12.34° and 24.64° 2θ . However, minor impurities, such as illite, muscovite and halloysite, also occur. Metakaolinite (Figure 2b) is characterized by the disappearance of all the XRD peaks of kaolinite, accompanied by the appearance of an amorphous aluminosilicate (see the broad hump at $2\theta = 13$ - 33° , having a maximum at $2\theta = \sim 22^{\circ}$). Similar results have been observed by as reported in several studies¹⁹⁻²¹.

Table 1. Synthesis conditions for transformation of kaolinite and metakaolinite into SOD and CAN zeotypes.

Chemical reagents				L/S ratio	Hydrothermal treatment		Molar gel composition
H ₂ O (mL)	NaOH (g)	KAO (g)	MTK (g)	(mL/g)	T ($^{\circ}\text{C}$)	t (hours)	
18.00	0.96	3.10		6.12	100	6	$\text{Na}_2\text{O}:\text{Al}_2\text{O}_3:2\text{SiO}_2:86.3\text{H}_2\text{O}$
18.00	0.96	3.10		6.12	100	72	$\text{Na}_2\text{O}:\text{Al}_2\text{O}_3:2\text{SiO}_2:86.3\text{H}_2\text{O}$
18.00	0.96	3.10		6.12	100	120	$\text{Na}_2\text{O}:\text{Al}_2\text{O}_3:2\text{SiO}_2:86.3\text{H}_2\text{O}$
18.00	2.87	3.10		6.73	100	6	$3\text{Na}_2\text{O}:\text{Al}_2\text{O}_3:2\text{SiO}_2:88.3\text{H}_2\text{O}$
18.00	2.87	3.10		6.73	100	72	$3\text{Na}_2\text{O}:\text{Al}_2\text{O}_3:2\text{SiO}_2:88.3\text{H}_2\text{O}$
18.00	2.87	3.10		6.73	100	120	$3\text{Na}_2\text{O}:\text{Al}_2\text{O}_3:2\text{SiO}_2:88.3\text{H}_2\text{O}$
18.00	0.96		2.67	7.10	100	22	$\text{Na}_2\text{O}:\text{Al}_2\text{O}_3:2\text{SiO}_2:84.2\text{H}_2\text{O}$
18.00	0.96		2.67	7.10	100	28	$\text{Na}_2\text{O}:\text{Al}_2\text{O}_3:2\text{SiO}_2:84.2\text{H}_2\text{O}$
18.00	0.96		2.67	7.10	100	52	$\text{Na}_2\text{O}:\text{Al}_2\text{O}_3:2\text{SiO}_2:84.2\text{H}_2\text{O}$

KAO, kaolinite; MTK, metakaolinite; L/S, alkaline solution/raw material ratio.

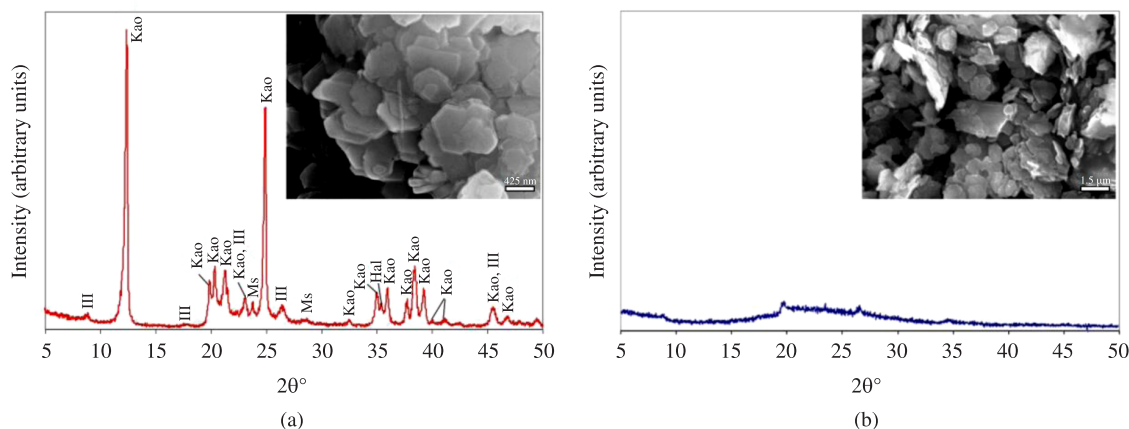


Figure 2. X-ray diffraction patterns and SEM images of the starting materials (a) kaolinite and (b) metakaolinite. Kao, Kaolinite; Ili, illite; Ms, muscovite; Hal, halloysite.

The SEM micrographs (Figure 2) reveals that kaolinite (Figure 2a) displays a platy morphology and hexagonal outlines, with small, well-formed hexagonal plates loosely packed, defining an orientation, whereas metakaolinite (Figure 2b) occurs as a mixture of large plates and stacks.

The FT-IR spectra of the starting materials (Figure 3) resemble those reported in previous studies. The vibration bands of kaolinite are described as follows. The band at 1119 cm^{-1} is referred to Si-O stretching vibrations, while the bands at 1034 and 1012 cm^{-1} are rather caused by Si-O-Si and Si-O-Al lattice vibrations²². The OH bending vibrations at 942 and 916 cm^{-1} can be referred to the 'surface OH bending' and 'inner OH bending'²³, which are mainly caused by Al-OH groups²². Further, bands in low range of frequency (762 , 696 and 539 cm^{-1}) can be attributed to different Si-O and Al-O vibrations²⁴. The conversion of kaolinite to metakaolinite is revealed by the disappearance of these characteristic bands, similar to what is reported in previous studies¹⁹⁻²⁰. The vibration bands observed in metakaolinite were 1049 , 806 , 642 , 571 and 428 cm^{-1} , with three broad bands centred at 1049 , 806 and 428 cm^{-1} . A significant shift of the Si-O vibration bands at 1034 and 1012 cm^{-1} in kaolinite to a higher frequency band at 1049 cm^{-1} was observed, which has been assigned to amorphous SiO_2 ^[25]. The stretching vibration of Al (O,OH)₆ octahedra in kaolinite²⁶ is observed at 539 cm^{-1} , but is substituted by a peak at 806 cm^{-1} corresponding to the vibration band of AlO_4 tetrahedron in metakaolinite.

The ^{29}Si MAS-NMR spectra of kaolinite and metakaolinite are given in Figure 4. The ^{29}Si MAS-NMR spectrum of kaolinite (Figure 4a) displays two well resolved signals at -90.9 and -91.4 ppm attributed to the existence of two different but equally populated silicon sites. Similar

results have been reported in several studies^{27,28}. According to Thompson and Barron¹²⁷, the interlayer hydrogen bonding resulting in two different silicon environments is the main reason for the ^{29}Si MAS-NMR signal splitting in kaolinite. The ^{29}Si MAS-NMR spectrum of metakaolinite (Figure 4b) displays a broad signal around -96.3 ppm , indicating its heterogeneity, with Si linked to four other Si atoms in silica polymorphs²⁹ and the presence of amorphous silica³⁰. According to Mackenzie et al.³¹, when kaolinite is dehydroxylated, the Si atoms undergo a range of environments of different distortion and the broadness of the metakaolinite line is attributed to these variations in the Si-O-Si(Al) bond angles. The ^{27}Al MAS-NMR spectrum of kaolinite (Figure 4a) consists of a sharp octahedral Al-O resonance at -3.4 ppm attributed to 6-coordinated Al. The ^{27}Al MAS-NMR spectrum of metakaolinite (Figure 4b) contains broad overlapping resonances at -0.3 , 23.4 and 45.9 ppm that can be attributed to 6-, 5- and 4-coordinated Al local environments, in agreement with data reported by Rocha³², although different compared with those reported by several authors^{30,33}. This reveals that the dehydroxylation of kaolinite brings about major changes, especially in the octahedral Al-O layers which are most closely associated with the structural hydroxyl groups³¹. The broader and asymmetrical peak shapes of metakaolinite show its disordered structure³³. However, it is very complicate to speculate on the metakaolinite structure, taking into account that there are a number of transitional stages, f,i, related to the temperature and duration of the kaolinite structure breakdown.

The thermal decomposition of kaolinite is illustrated in the TG and its first derivative (DTG) curves on Figure 5. At $<100\text{ }^\circ\text{C}$, low temperature release of absorbed water occurs.

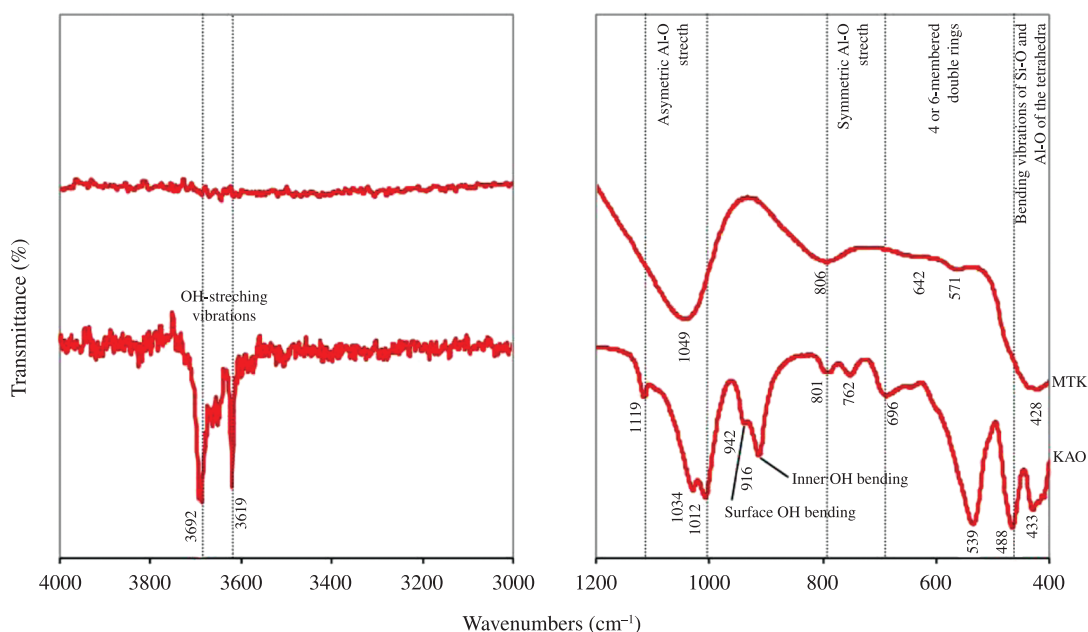


Figure 3. FTIR spectra of the starting materials. KAO, kaolinite; MTK, metakaolinite.

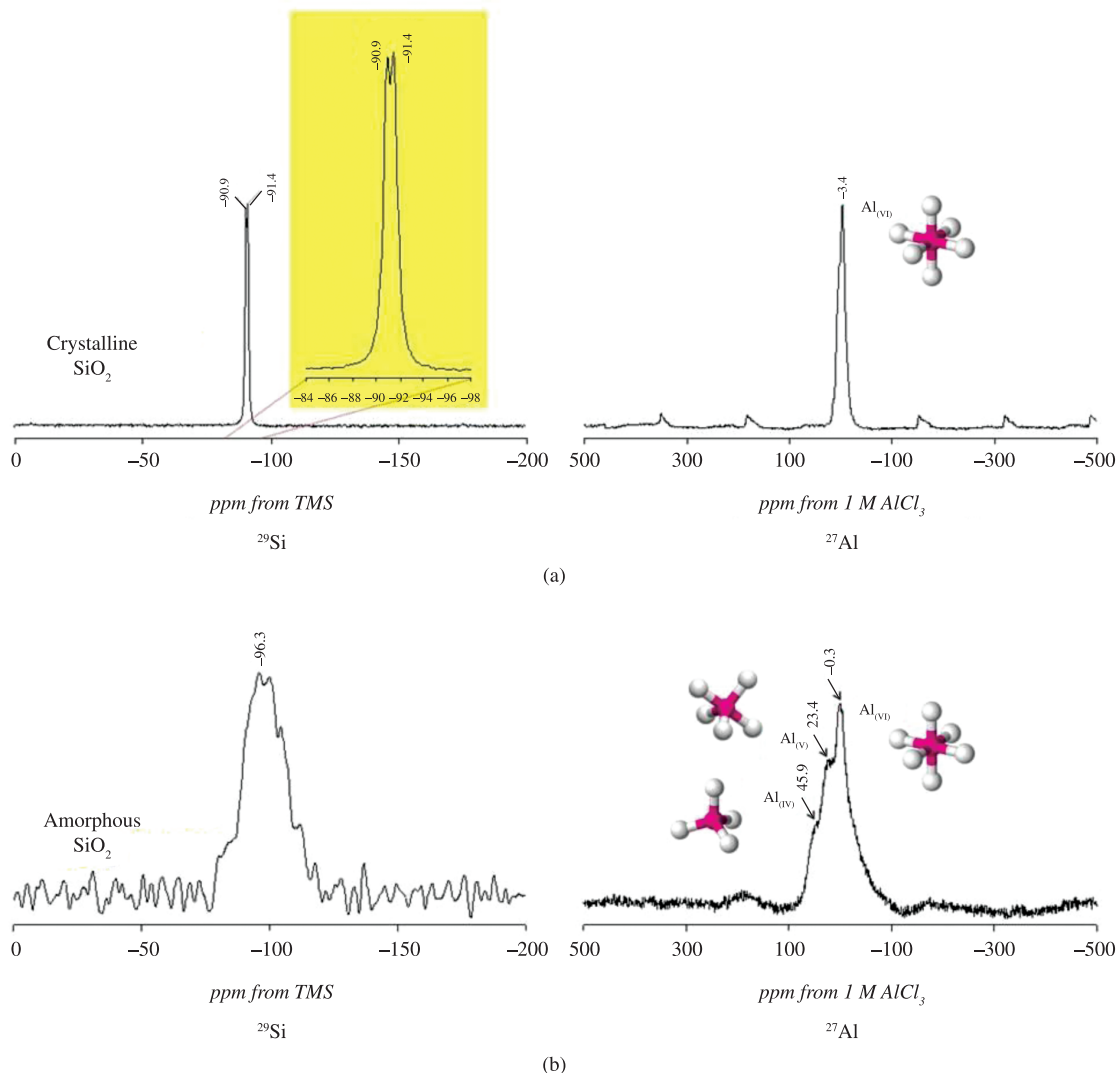


Figure 4. Solid-state ^{29}Si and ^{27}Al MAS-NMR spectra of the starting materials: (a) kaolinite and (b) metakaolinite.

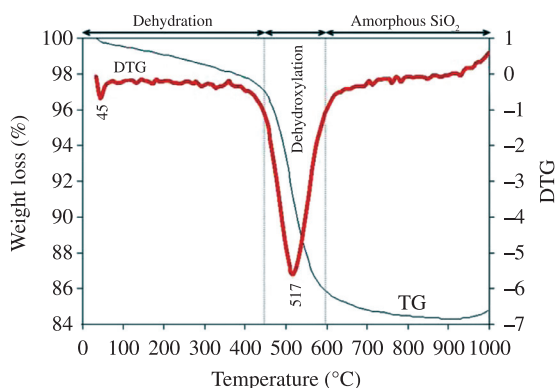


Figure 5. TG/DTG curves between 25-1000 °C for kaolinite.

Between ~100-450 °C, a pre-dehydration process takes place as a result of the reorganization in the octahedral layer, first occurring at the OH of the surface³⁴. After dehydration,

kaolinite undergoes a pre-dehydroxylation state³⁵. Between ~450-600 °C, the kaolinite dehydroxylation occurs, with the transformation to a non-crystalline phase, metakaolinite. According to Varga³⁶, the transformation of kaolinite into metakaolinite by dehydroxylation results in structural disturbances through the breaking of unstable bonds. As a result, the degree of ordering became lower than that in kaolinite as dehydroxylation progressed. The structure of metakaolinite does not collapse but, rather, retains a layered structure. A progressive decomposition of the metakaolinite occurs up to 900 °C. An exothermic peak at ~1000 °C reveals the breakdown of the metakaolinite structure and the formation of mullite or Si-Al spinel with mullite-like composition, as reported by Chakravorty and Ghosh³⁷.

3.2. As-synthesized zeotypes

3.2.1. XRD analysis

As mentioned before, the structural frameworks of both SOD and CAN are similar. As a result many diffraction peaks

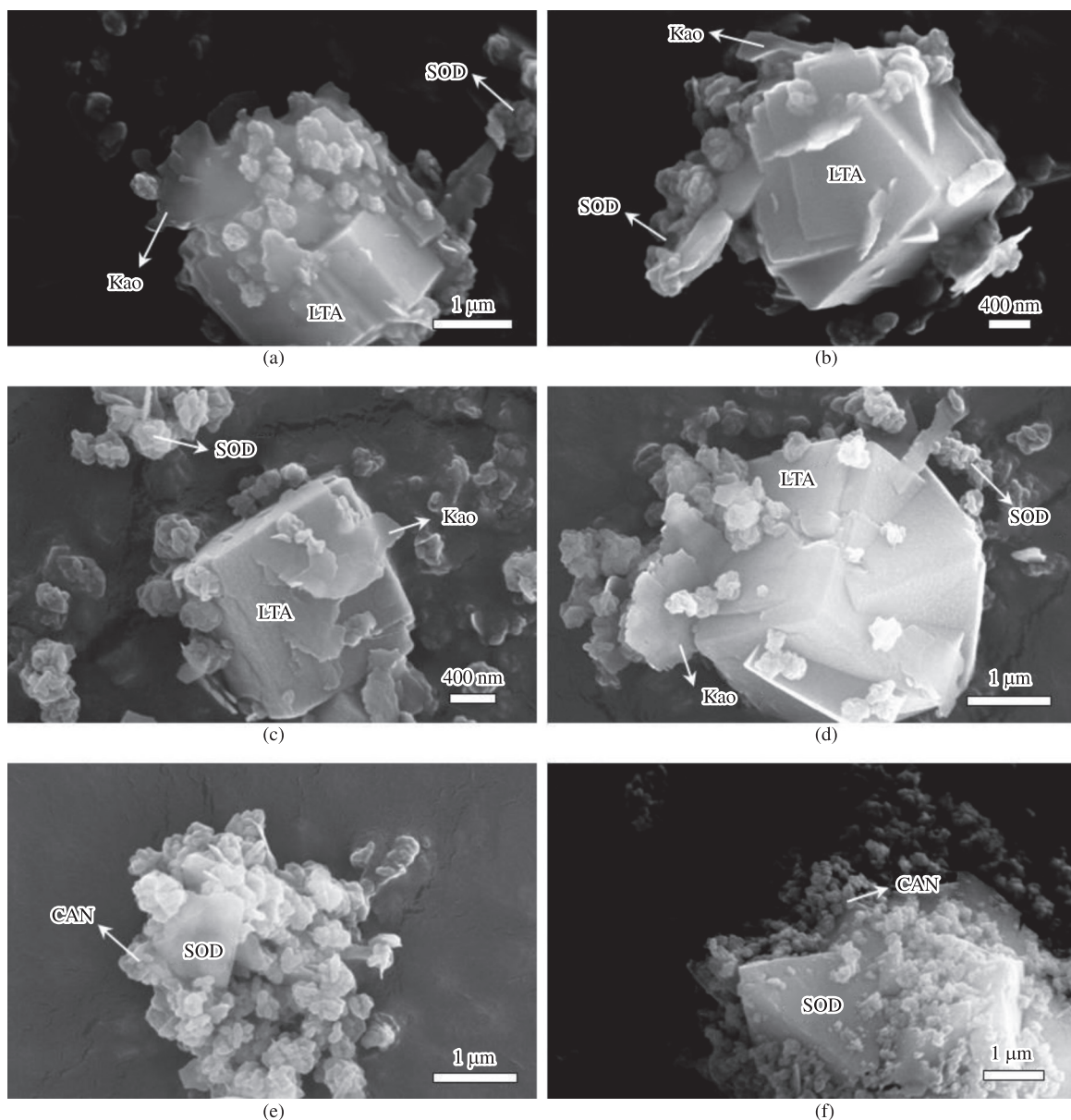


Figure 7. SEM images showing several synthesis products obtained by hydrothermal treatment of the starting kaolinite in (a)(b) 1.33 M NaOH solutions, after 6 hours of reaction at 100 °C, (c)(d) 1.33 M NaOH solutions, after 120 hours of reaction at 100 °C, and (e) (f) 3.99 M NaOH solutions, after 120 hours of reaction at 100 °C.

vibrations for SOD and CAN in this range. Coincident with the disappearance of kaolinite, characteristic zeolite bands appeared on the spectra, including the asymmetric Al-O stretch located in the region of 1250-950 cm^{-1} , and their symmetric Al-O stretch located in the region of 770-660 cm^{-1} . The region 1200-850 cm^{-1} shows a single vibration band centred at 960-965 cm^{-1} , associated with the presence of CAN. The transmittance of the asymmetric stretch of the Si-O-Al in the SOD framework consists of a single band at 980 cm^{-1} , which split into four bands at 1110, 1050, 1020, and 960 cm^{-1} assigned to CAN⁴. However, this study reports only the bands at 975 and 960-965 cm^{-1} , corresponding to SOD and CAN, respectively. The region

850-750 cm^{-1} reveals a weak vibration band at 766-768 cm^{-1} , characteristic of CAN. Several bands in the region 750-650 cm^{-1} indicate the presence of a mixture of SOD and CAN in the as-synthesized products. The bands in the region 650-500 cm^{-1} are related to the presence of the double rings (D4R and D6R) in the framework structures of the zeolitic materials⁹. The bands in the region 500-420 cm^{-1} are related to internal tetrahedron vibrations of Si-O and Al-O of the zeotypes. The region 800-400 cm^{-1} can be considered as the fingerprint region for zeolite LTA, SOD, and CAN as suggested in previous studies^{4,41}. As shown in Figure 9b, The characteristic vibration bands of metakaolinite disappeared, accompanied by the appearance of new peaks that reveal

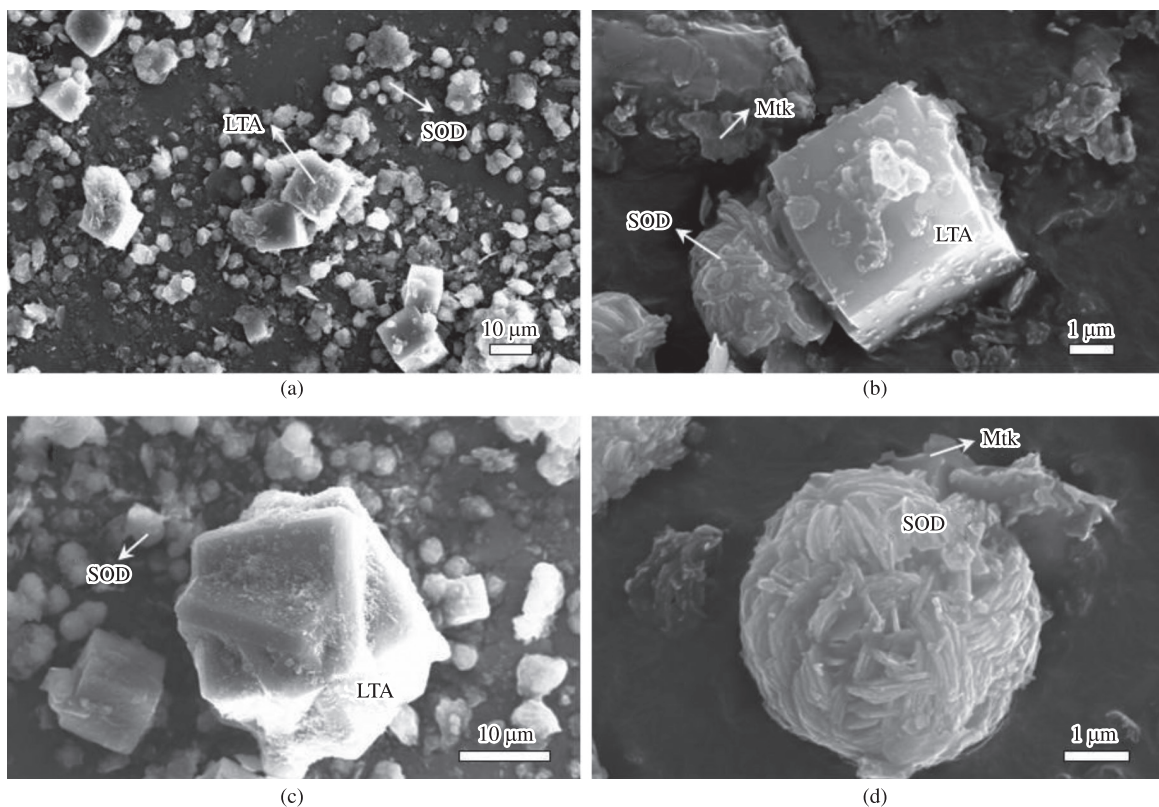


Figure 8. SEM images showing several synthesis products obtained by hydrothermal treatment of the starting metakaolinite in (a)(d) 1.33 M NaOH solutions, after 52 hours of reaction at 100 °C.

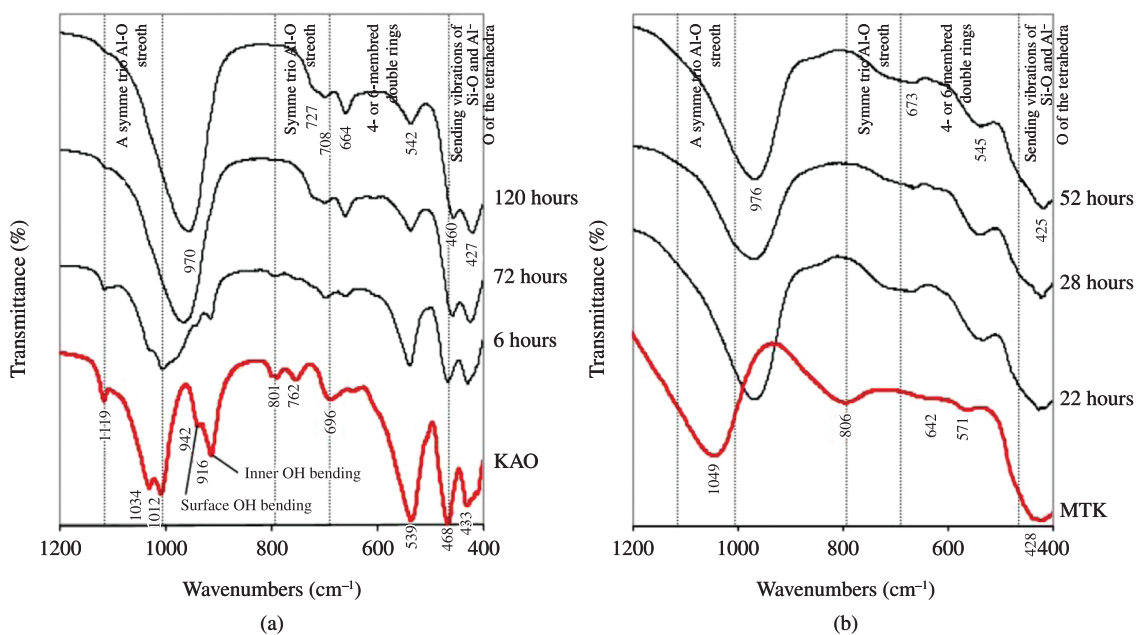


Figure 9. FTIR spectra of unreacted raw materials and the as-synthesized zeotypes obtained after hydrothermal transformation of (a) kaolinite and (b) metakaolinite in 1.33 M NaOH solutions at 100 °C after several reaction times.

the occurrence of zeolite LTA. The band at 1047 cm^{-1} was shifted to lower frequency bands (at $973\text{--}980\text{ cm}^{-1}$); the band at 800 cm^{-1} disappeared in the zeolitic products; the low intensity bands at 635 and 565 cm^{-1} were shifted to higher (at $673\text{--}690\text{ cm}^{-1}$) and lower (at $530\text{--}538\text{ cm}^{-1}$) frequency bands, respectively. The band at 424 cm^{-1} was shifted to lower frequency bands (at $411\text{--}417\text{ cm}^{-1}$). The typical bands of zeolite LTA representing the asymmetric Al-O ($973\text{--}980\text{ cm}^{-1}$) and symmetric Al-O ($673\text{--}690\text{ cm}^{-1}$) stretches, double rings ($530\text{--}538\text{ cm}^{-1}$) in the framework structures of the zeolitic materials were observed and they show a constant intensity. The FT-IR peak width is an indication of the level of the crystallinity of the synthesis products.

3.2.4. ^{29}Si and ^{27}Al MAS-NMR

Figure 10 shows the ^{29}Si and ^{27}Al MAS-NMR spectra of the starting kaolinite and representative as-synthesized zeotypes. The ^{29}Si MAS-NMR spectrum of the synthesis products show three resonances at -83.6 , -86.3 and -91.2 ppm. The chemical shifts at -83.6 and -86.3 ppm can be attributed to $\text{Q}^4(4\text{Al})$ environments in SOD and CAN⁴³. The presence of the two Si sites indicates imperfect Al/Si ordering in tetrahedral sites. CAN was reported to have a chemical shift of -87.3 ppm⁴. Therefore, in this study the signal at -86.3 ppm can be presumably attributed to CAN. In some studies, ^{29}Si MAS-NMR has been used to differentiate between SOD and CAN^{44,45}. However, according to Barnes et al.⁴, no difference in chemical shift between these zeotypes can be recognized in terms of ^{29}Si MAS-NMR. The -91.2 ppm chemical shift can be assigned

to the presence of residual kaolinite. The ^{27}Al MAS-NMR spectrum of the synthesis products shows a single resonance at 59.5 ppm, which can be assigned to tetrahedral Al in the framework of the zeotypes, but with some octahedral Al corresponding to the presence of residual kaolinite. The reaction of the kaolinite with NaOH as mineralizer resulted in a shift of Al from octahedral to tetrahedral coordination, which is likely due to the dissolution of this clay mineral and the subsequent precipitation of the zeotypes. The amount of Al(6) is greatest in kaolinite (Figure 10a) where the initial Al concentration was larger compared with that in the synthesis products (Figure 10b). The decrease in the Al(6)/Al(4) ratio can be explained by the dissolution of kaolinite, with Al coordination changing from octahedral to tetrahedral, which is consistent with the formation of zeolite-type materials.

Figure 11 shows the ^{29}Si and ^{27}Al MAS-NMR spectra of the starting metakaolinite and representative as-synthesized zeotypes. The ^{29}Si MAS-NMR spectrum of the synthesis products shows a sharp signal at -89.5 ppm, which is characteristic of $\text{Q}^4(4\text{Al})$ sites in zeolite LTA, similar to that observed by Akolekar et al.²⁰. A weak signal at -85.9 ppm can be attributed to the contribution of $\text{Q}^4(4\text{Al})$ sites of SOD and CAN. ^{29}Si MAS-NMR results point out the change of the silica morphology from amorphous SiO_2 in the metakaolinite to crystalline SiO_2 in the zeotypes, with the total dissolution of the starting metakaolinite to form zeolite-type structures and the incorporation of aluminium. The ^{27}Al MAS-NMR spectrum of the synthesis products shows a single resonance at 58.2 ppm, which can be assigned to tetrahedral Al in the zeotypes.

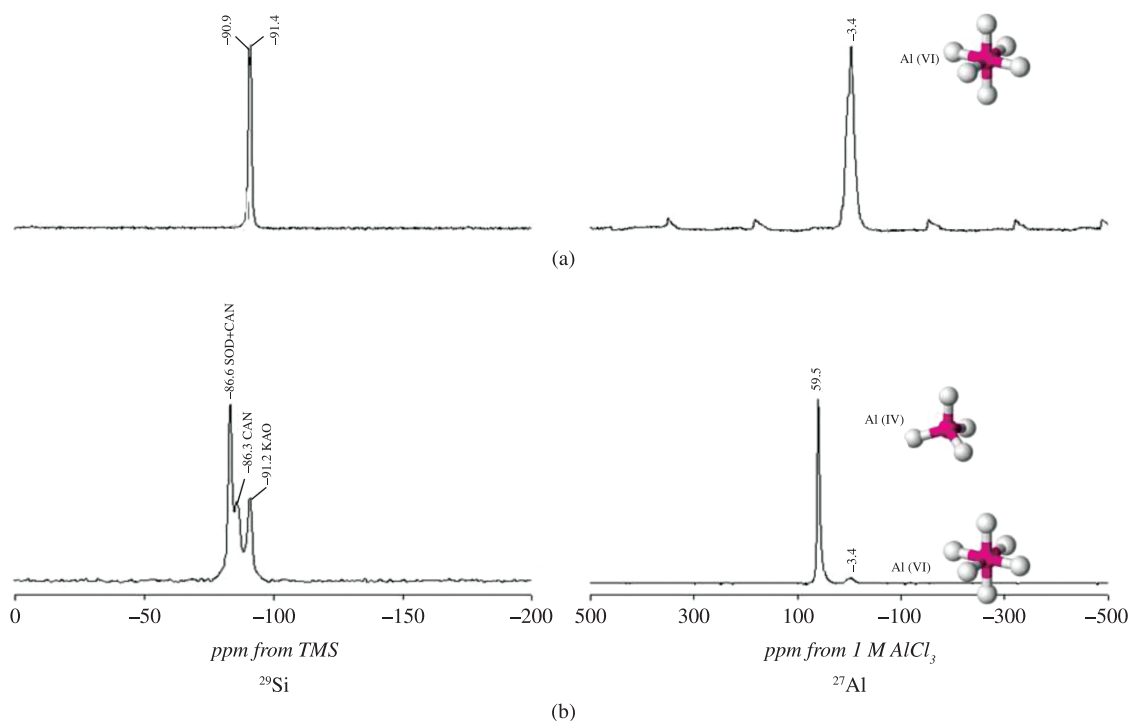


Figure 10. ^{29}Si and ^{27}Al MAS-NMR spectra of the (a) starting kaolinite and (b) representative as-synthesized zeotypes obtained after hydrothermal transformation of kaolinite in 1.33 M NaOH solutions at $100\text{ }^\circ\text{C}$ after 120 hours of reaction.

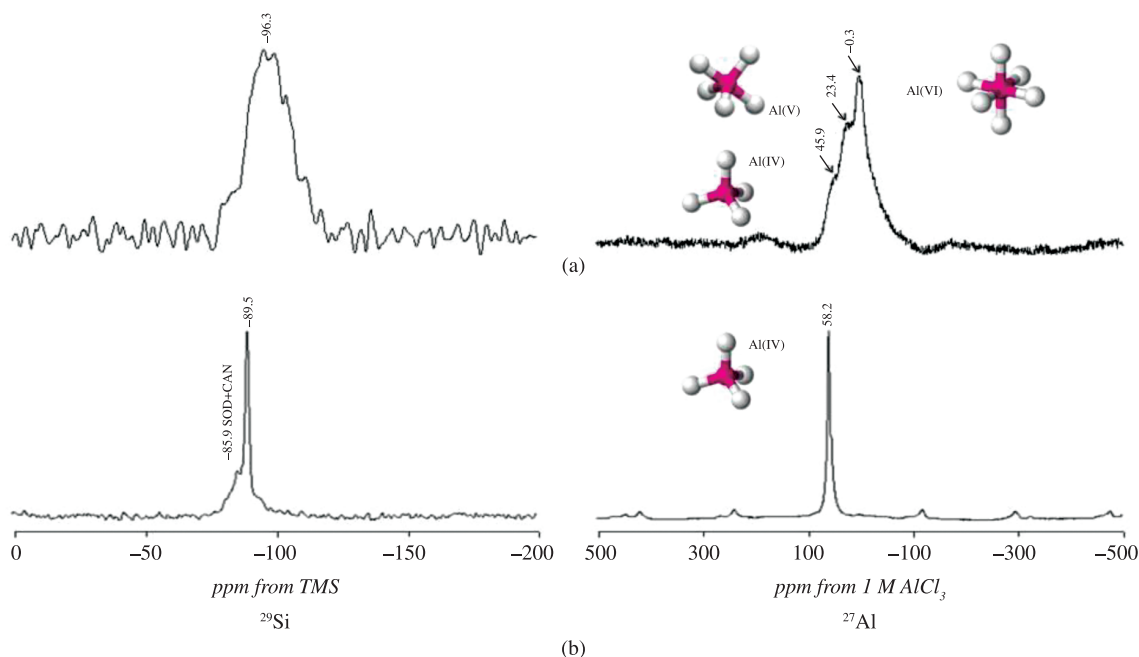


Figure 11. ^{29}Si and ^{27}Al MAS-NMR spectra of the (a) starting metakaolinite and (b) representative as-synthesized zeotypes obtained after hydrothermal transformation of metakaolinite in 1.33 M NaOH solutions at 100 °C after 52 hours of reaction.

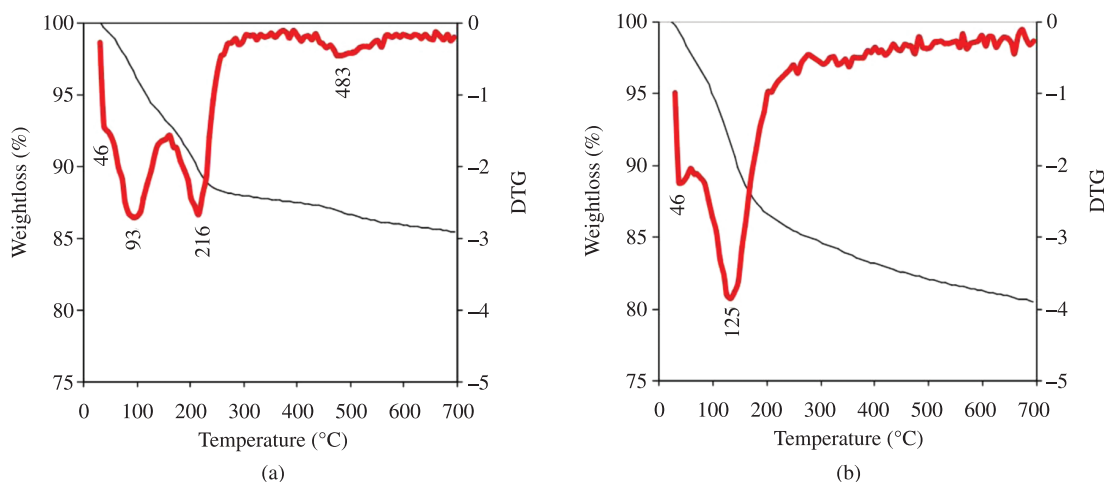


Figure 12. TG/DTG curves from 25 to 700 °C of the representative as-synthesized zeotypes obtained after hydrothermal transformation of (a) kaolinite and (b) metakaolinite in 1.33 M NaOH solutions at 100 °C after 120 hours and 52 hours of reaction, respectively.

3.2.5. TG analysis

DTG curves of the representative as-synthesized zeotypes are shown in Figure 12. The synthesis products show up to four dehydration steps. The position of these DTG peaks and the number of dehydration steps can be attributed to the different compensating cation-water binding energies as well as to the different energy associated with the diffusion of the desorbed water through the porous structure of the as-synthesized products; their weight loss percentages reflects the water loss from the zeolite structure, and the amount of desorbed water is related with the number

of compensation cations in the framework of the zeolite⁴⁶. The peaks observed between 39–52 °C correspond to surface water in zeolitic materials; the peaks observed between 100–162 °C indicate zeolitic water, although in some cases in this temperature range up to two peaks occur, which can be explained by the heterogeneous nature of the as-synthesized products.

3.3. Phase transformation from SOD to CAN

The SOD and CAN zeotypes present a ratio of Si/Al = 1, being one of the few structures that have compensation

anions⁴⁷. Therefore, it is not surprising that they can be synthesized under similar conditions. The formation of a specific structure (SOD-type or CAN-type), depends on, among other factors, the symmetry, the charge of the anion and the basicity of the medium⁴⁷. Walton et al.⁴⁸ studied on the influence of the reaction condition of the hydrothermal crystallization and the transformation of zeolite LTA into SOD by time resolved in situ energy dispersive X ray diffraction.

According to Barnes et al.², the phase transformation from SOD to CAN was a solution-mediated process, which involved a four-stage mechanism: (1) dissolution of SOD, (2) relative CAN supersaturation as a result of SOD dissolution, (3) nucleation of CAN, and (4) simultaneous growth of CAN nuclei and dissolution of SOD.

Results from this study are in agreement with regard to SOD forms first and then transforms slowly to CAN at a rate that increases with increasing temperature^{4,17}. Consequently, the formation of these aluminosilicate phases may be considered as being dominated by kinetics rather than thermodynamics².

A mixture of LTA zeolite, SOD, and CAN was obtained at 100 °C, as demonstrated by XRD patterns shown in Figure 2. The formation of these zeolitic materials is in agreement with the previous study by Ríos et al.¹⁴, which suggest that zeolite LTA is the main zeolitic phase at shorter reaction times, whereas SOD- and CAN-type structures were formed from hydrogels at longer reaction times.

3.4. Nucleation and growth process of SOD and CAN

During recent years, several research groups have made great efforts to successfully bridge the gap between the general formation mechanisms of crystalline phases and the crystallization of complex structures, such as those of zeolites⁴⁹. However, specific information concerned with crystallization mechanism and kinetics is limited⁹. The chemistry of evolution of relatively simple zeolite systems, can be affected by several factors, such as the formation of intermediate metastable phases (e.g. zeolite LTA), the occurrence of simultaneous reactions such as precipitation and dissolution of a gel phase, nucleation and growth of zeotypes, dissolution of the early metastable phases, nucleation and growth of more stable phases such as SOD and CAN, with a dissolution of the initial crystals, and nucleation and growth of the crystalline phases that reached chemical equilibrium. However, the reaction history of the zeolite synthesis developed in this study can be summarized as follows.

The process of synthesis can be described by two main stages: (1) the dissolution of aluminosilicate compounds releasing Si and Al and (2) the zeolite crystallization. Zeolites are typically crystallized from amorphous aluminosilicate precursors in aqueous in the presence of alkali metals. A simple scheme of the crystallization of an amorphous aluminosilicate hydrogel to SOD and CAN is given in Figure 13.

At the beginning of the synthesis process, a dissolution of the starting materials occurred, with the production of an amorphous gel characterized by the presence of small

oligomers (Figure 13a). A dissolution process promotes the formation of the nutrients (ionic species) which then are transported to the nucleation sites, indicating that the ionic species are not static, because they necessarily need to move (transportation) to the nucleation sites. A nucleation process (Figure 13b) produced an equilibrated gel. During nucleation, hydrogel composition and structure are significantly affected by thermodynamic and kinetic parameters. A polymerization of SiO₄ tetrahedra proceed (Figure 13c), which is represented by TO₄ primary tetrahedral building units have been joined, revealing how they link together to form larger structures. A polymerization is the process that forms the zeolite precursors, which contains tetrahedral of Si and Al randomly distributed along the polymeric chains that are cross-linked so as to provide cavities large enough to accommodate the charge balancing alkali ions. During crystal growth (Figure 13d) the TO₄ units were linked, with the formation of 4-ring and 6-ring, composed by 4 and 6 tetrahedral atoms, respectively, to create a large structure (secondary building unit) like the SOD β -cage. The crystallization of zeolite LTA occurred by linking the same secondary building units together (Figure 13e). A phase transformation occurred as represented by the sequence of reaction: zeolite LTA \rightarrow SOD \rightarrow CAN (Figure 13f).

According to Breck⁹, the hydrogel composition and structure is controlled by the size and structure of the polymerization species and gelation controls the nucleation of the zeolite crystallites, which is supported by the crystal size and morphology of zeolites grown from hydrogels. It is clear from data reported by Barnes et al.² that at lower temperature and NaOH concentration than those used in this study zeolite LTA transforms to zeolite P. We consider that SOD should appear after zeolite LTA without the formation of zeolite P. However, Ríos¹⁵ reported the co-crystallization of SOD + CAN, which was followed by the crystallization of the JBW-type structure at higher temperature and NaOH concentration. Ogura et al.⁵⁰ reported that cyclic tetramer and hexamer species could be found in the liquid phase to generate SOD cages. SOD nucleated homogeneously in the liquid phase and grown without intervention of hydrogel⁵¹. On the other hand, results reported by Lee et al.⁵¹ clearly explain that SOD crystallization takes place by the solid-solid transformation without involving any solution or amorphous-mediated process. However, the transformation of SOD to CAN involves a solution-mediated mechanism with SOD dissolution and subsequent CAN precipitation as suggested by Barnes et al.². They also demonstrated that CAN is formed at expense of two dimorphs of cubic SOD, which show a notable change in unit cell size as reported by Zheng et al.¹⁷.

The mineral transformations and the stability of the end products were controlled by experimental parameters like NaOH concentration, temperature and Si/Al ratio. However, they were likely affected by several factors, such as the formation of intermediate metastable phases and the occurrence of different chemical processes, including precipitation and dissolution of a gel phase, nucleation and growth of zeotypes, dissolution of the early metastable phases, nucleation and growth of more stable phases (SOD

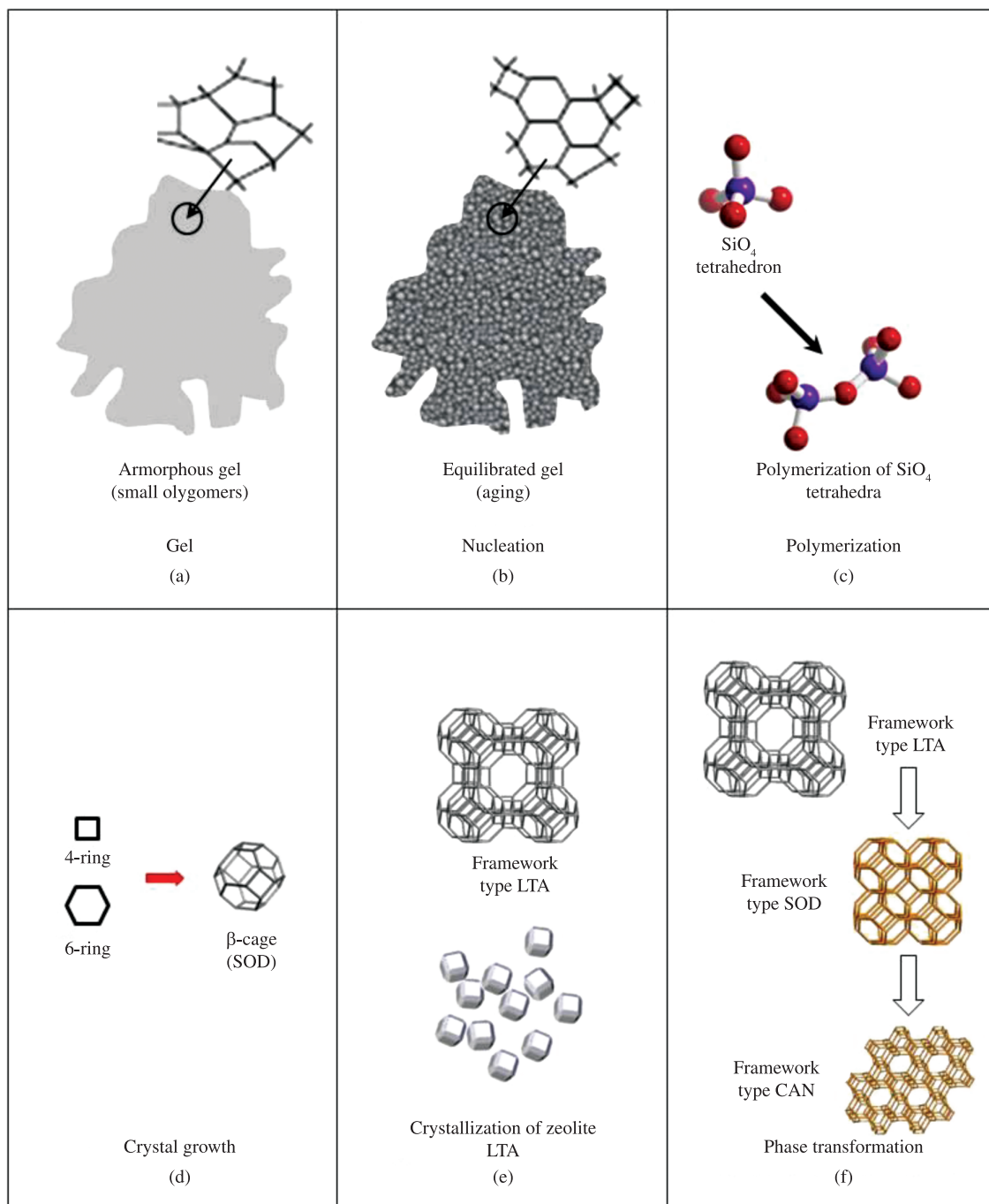


Figure 13. Illustration of the proposed sequence for the formation of zeotypes.

and CAN), with a dissolution of the initial crystals and nucleation and growth of the crystalline phases that reached chemical equilibrium.

Ríos et al.^{6,14,15} have demonstrated that the occurrence of a sequence of chemical reactions from amorphous aluminosilicate gel to crystalline zeotypes, which can be summarized as follows:

Poorly crystalline aluminosilicate \rightarrow zeolite LTA \rightarrow SOD \rightarrow SOD + CAN \rightarrow CAN.

The hydrothermal transformation of the starting kaolinite and metakaolinite at low temperature presumably reveals a similar sequence of reactions, starting with an amorphous material after dissolution of the aluminosilicate phases, followed by zeolite LTA as the first and metastable phase formed, SOD-type structure, a mixture of SOD-type and CAN-type structures and finally CAN (apparently more stable than SOD) as the stable and final synthesis product. However, according to Barnes et al.², CAN appeared more

stable than SOD, concluding that CAN would be the final product, whereas amorphous material, zeolite LTA and SOD would be transition phases. Fechtelkord et al.⁵² argued that SOD is the thermodynamically more stable phase and CAN formation is kinetically favored at lower NaOH concentrations. Similar results can be assumed in this study. We are in agreement with the fact that these phase transformations did not occur in the solid state and, therefore, represent a solution-mediated mechanism as suggested by previous studies^{2,39}. According to XRD data a co-crystallization of zeolite LTA, SOD and CAN occurs, being very difficult to evaluate phase transformations due to the very constant behaviour of the XRD peaks of these zeotypes and to the overlapping of peaks of SOD-type and CAN-type structures, which makes difficult to quantifying SOD and CAN mixtures. However, SEM data reveal phase relationships in which (1) lepispheric aggregates of SOD and CAN grow onto the surface of cubic crystals of zeolite LTA or (2) CAN grows at the expense of SOD. Under the experimental conditions considered by Deng et al.³⁹ there is enough evidence about phase transformations that occur in this chemical system. However, in this study a slight higher temperature (100 °C) was used, which can explain why zeolite LTA (a metastable phase) occurs as a minor phase, compared with the presence of SOD and CAN.

4. Conclusions

Zeotypes such as SOD and CAN were successfully synthesized via hydrothermal treatment using kaolinite and metakaolinite as starting materials and NaOH as activating agent. However, zeotype formation was assessed to be fairly

unsuccessful via zeolite LTA, taking into account that the synthesis products area characterized by the occurrence of SOD and CAN as metastable phases. The structural similarity between zeolites and feldspathoids explain why they can coexist in the as-synthesized products and the dominant crystalline phase depends on formation conditions. The main crystalline phases obtained after synthesis process were zeolite LTA, SOD and CAN. The synthesis products are strongly controlled by the starting material, taking into account that metakaolinite is a more reactive phase than kaolinite. There were two major chemical processes involved in the reaction between the starting kaolinite and metakaolinite and alkaline solutions: dissolution of the starting materials followed by the formation of zeolitic materials. Future research, should consider to develop further experiments under well-optimized conditions for obtaining individual phases instead of mixtures, and evidently in order to clarify the sequence of phase crystallization.

5. Acknowledgements

We thank the Programme Alban, the European Union Programme of High Level Scholarships for Latin America, scholarship No. E05D060429CO, and the Universidad Industrial de Santander for funding C.A. Ríos. Special thanks to School of Applied Sciences at University of Wolverhampton for allowing us the use of the research facilities. We thank Dr Townrow and Mrs Hodson for assistance in collecting XRD and SEM data, respectively, and Dr Apperley at the University of Durham for MAS-NMR spectra.

References

- Barnes MC, Addai-Mensah J and Gerson AR. The solubility of sodalite and cancrinite in synthetic spent Bayer liquor. *Colloids and Surfaces A: Physicochemical and Engineering Aspects*. 1999; 157:106-116. [http://dx.doi.org/10.1016/S0927-7757\(99\)00058-8](http://dx.doi.org/10.1016/S0927-7757(99)00058-8)
- Barnes MC, Addai-Mensah J and Gerson AR. The mechanism of the sodalite-to-cancrinite phase transformation in synthetic spent Bayer liquor. *Microporous and Mesoporous Materials*. 1999; 31:287-302. [http://dx.doi.org/10.1016/S1387-1811\(99\)00079-7](http://dx.doi.org/10.1016/S1387-1811(99)00079-7)
- Xu B, Smith P, Wingate C and De Silva L. The effect of calcium and temperature on the transformation of sodalite to cancrinite in Bayer digestion. *Hydrometallurgy*. 2010; 105:75-81. <http://dx.doi.org/10.1016/j.hydromet.2010.07.010>
- Barnes MC, Addai-Mensah J and Gerson AR. A methodology for quantifying sodalite and cancrinite phase mixtures and the kinetics of the sodalite to cancrinite phase transformation. *Microporous and Mesoporous Materials*. 1999; 31:303-319. [http://dx.doi.org/10.1016/S1387-1811\(99\)00080-3](http://dx.doi.org/10.1016/S1387-1811(99)00080-3)
- Barrer RM. *Zeolites and Clay Minerals as Sorbents and Molecular Sieves*. London: Academic Press; 1978.
- Ríos CA, Williams C and Fullen MA. Nucleation and growth history of zeolite LTA synthesized from kaolinite by two different methods. *Applied Clay Science*. 2009; 42:446-454. <http://dx.doi.org/10.1016/j.clay.2008.05.006>
- Zeolite Structures. *Database*. Available from: <<http://www.iza-structure.org/databases/>>.
- Heller-Kallai L and Lapidés I. Reactions of kaolinites and metakaolinites with NaOH - Comparison of different samples (Part 1). *Applied Clay Science*. 2007; 35:99-107. <http://dx.doi.org/10.1016/j.clay.2006.06.006>
- Breck DW. *Zeolite Molecular Sieves: Structure, Chemistry and Use*. New York: John Wiley; 1974.
- Chandrasekhar S and Pramada PN. Investigation on the synthesis of zeolite NaX from Kerala kaolin. *Journal of Porous Materials*. 1999; 6:283-297. <http://dx.doi.org/10.1023/A:1009632606671>
- Mackenzie RC. *Differential Thermal Analysis 1*. London: Academic Press; 1970.
- Rocha J, Klinowski J and Adams JM. Synthesis of zeolite Na-A from metakaolinite revisited. *Journal of the Chemical Society, Faraday Transactions*. 1991; 87:3091-3097. <http://dx.doi.org/10.1039/ft9918703091>
- Lapidés I and Heller-Kallai L. Reactions of metakaolinite with NaOH and colloidal silica - Comparison of different samples (Part 2). *Applied Clay Science*. 2007; 35:94-98. <http://dx.doi.org/10.1016/j.clay.2006.06.007>
- Ríos CA, Williams CD and Maple MJ. Synthesis of zeolites and zeotypes by hydrothermal transformation of kaolinite and metakaolinite. *Bistua*. 2007; 5:15-26.

15. Ríos CA. *Synthesis of zeolites from geological materials and industrial wastes for potential application in environmental problems*. [Thesis]. Wolverhampton: University of Wolverhampton; 2008.
16. Zheng K, Smart RSC, Addai-Mensah J and Gerson AR. The solubility of sodium aluminosilicates in synthetic Spent Bayer liquor. *Journal of Chemical & Engineering Data*. 1998; 43:312-317. <http://dx.doi.org/10.1021/jc970187i>
17. Zheng K, Gerson AR, Addai-Mensah J and Smart RSC. The influence of sodium carbonate on aluminosilicate crystallization and solubility in sodium aluminate solutions. *Journal of Crystal Growth*. 1997; 171:197-208. [http://dx.doi.org/10.1016/S0022-0248\(96\)00480-0](http://dx.doi.org/10.1016/S0022-0248(96)00480-0)
18. Breuer RG and Barsotti LR. Kelly AC. Extractive Metallurgy of Aluminium. *Interscience*. 1963; 7:133-157.
19. Zhao H, Deng Y, Harsh JB, Flury M and Boyle JS. Alteration of Kaolinite to Cancrinite and Sodalite by Simulated Hanford Tank Waste and its impact on Cesium retention. *Clays and Clay Minerals*. 2004; 52:1-13. <http://dx.doi.org/10.1346/CCMN.2004.0520101>
20. Akolekar D, Chaffee A and Howe RF. The transformation of kaolin to low-silica X zeolite. *Zeolites*. 1997; 19:359-365. [http://dx.doi.org/10.1016/S0144-2449\(97\)00132-2](http://dx.doi.org/10.1016/S0144-2449(97)00132-2)
21. Murat M, Amokrane A, Bastide JP and Montanaro L. Synthesis of zeolites from thermally activated kaolinite. Some observations on nucleation and growth. *Clay Minerals*. 1992; 27:119-130. <http://dx.doi.org/10.1180/claymin.1992.027.1.12>
22. Van der Marel HW and Beutelspacher H. *Atlas of Infrared Spectroscopy of Clay Minerals and Their Admixtures*. Amsterdam: Elsevier; 1976.
23. Frost RL, Mako E, Krsitof J and Klopogge JT. Modification of kaolinite surfaces through mechanochemical treatment - a mid-IR and near-IR spectroscopic study. *Spectrochimica Acta Part A: Molecular and Biomolecular Spectroscopy*. 2002; 58:2849-2859. [http://dx.doi.org/10.1016/S1386-1425\(02\)00033-1](http://dx.doi.org/10.1016/S1386-1425(02)00033-1)
24. Hoch M and Bandara A. Determination of the adsorption process of tributyltin (TBT) and monobutyltin (MBT) onto kaolinite surface using Fourier transform infrared (FT-IR) spectroscopy. *Colloids and Surfaces A: Physicochemical and Engineering Aspects*. 2005; 253:117-124. <http://dx.doi.org/10.1016/j.colsurfa.2004.10.118>
25. Qiu G, Jiang T, Li G, Fan X and Huang Z. Activation and removal of silicon in kaolinite by thermochemical process. *Scandinavian Journal of Metallurgy*. 2004; 33:121-128. <http://dx.doi.org/10.1111/j.1600-0692.2004.00677.x>
26. Lambert JF, Minman WS and Fripiat JJ. Revisiting kaolinite dehydroxylation: A silicon-29 and aluminum-27 MAS NMR study. *Journal of the American Chemical Society*. 1989; 111:3517-3522. <http://dx.doi.org/10.1021/ja00192a005>
27. Thompson JG and Barron PF. Further consideration of the ^{29}Si nuclear magnetic resonance spectrum of kaolinite. *Clays and Clay Minerals*. 1987; 35:38-42. <http://dx.doi.org/10.1346/CCMN.1987.0350105>
28. Letaief S, Elbokl TA and Detellier C. Reactivity of ionic liquids with kaolinite: Melt intersalation of ethyl pyridinium chloride in an urea-kaolinite pre-intercalate. *Journal of Colloid and Interface Science*. 2006; 302:254-258. <http://dx.doi.org/10.1016/j.jcis.2006.06.008>
29. Smith JV and Blackwell CS. Nuclear magnetic resonance of silica polymorphs. *Nature*. 1983; 303:223-225. <http://dx.doi.org/10.1038/303223a0>
30. Rocha J and Klinowski J. ^{29}Si and ^{27}Al magic-angle-spinning NMR studies of the thermal transformation of kaolinite. *Physics and Chemistry of Minerals*. 1990; 17:179-186.
31. Mackenzie KJD, Brown IWM, Meinhold RH and Bowden ME. Outstanding problems in the kaolinite-mullite reaction sequence investigated by ^{29}Si and ^{27}Al Solid-State Nuclear Magnetic Resonance: I. Metakaolinite. *Journal of the American Ceramic Society*. 1985; 68:293-297. <http://dx.doi.org/10.1111/j.1151-2916.1985.tb15228.x>
32. Rocha R. Single- and triple-quantum ^{27}Al MAS NMR study of the thermal transformation of kaolinite. *Journal of Physical Chemistry B*. 1999; 103:9801-9804. <http://dx.doi.org/10.1021/jp991516b>
33. Liu Q, Spears DA and Liu Q. MAS NMR study of surface-modified calcined kaolin. *Applied Clay Science*. 2001; 19:89-94. [http://dx.doi.org/10.1016/S0169-1317\(01\)00057-6](http://dx.doi.org/10.1016/S0169-1317(01)00057-6)
34. Balek V and Murat M. The emanation thermal analysis of kaolinite clay minerals. *Thermochimica Acta*. 1996; 282-283:385-397. [http://dx.doi.org/10.1016/0040-6031\(96\)02886-9](http://dx.doi.org/10.1016/0040-6031(96)02886-9)
35. Frost RL, Horváth E, Makóc E, Kristóf J and Rédey A. Slow transformation of mechanically dehydroxylated kaolinite to kaolinite - an aged mechanochemically activated formamide - intercalated kaolinite study. *Thermochimica Acta*. 2003; 408:103-113. [http://dx.doi.org/10.1016/S0040-6031\(03\)00316-2](http://dx.doi.org/10.1016/S0040-6031(03)00316-2)
36. Varga G. The structure of kaolinite and metakaolinite. *Építőanyag*. 2007; 59:4-8.
37. Chakravorty AK and Ghosh DK. Kaolinite-mullite reaction series: The development and significance of a binary aluminosilicate phase. *Journal of the American Ceramic Society*. 1991; 74:1401-1406. <http://dx.doi.org/10.1111/j.1151-2916.1991.tb04119.x>
38. Subotic B, Masic N and Smit I. Analysis of Particulate Processes During the Transformation of Zeolite A into Hydroxysodalite. In: Drzaj B, Hocevar S and Pejovnik S, editors. *Zeolites - Synthesis, Structure, Technology and Application Studies in Surface Science and Catalysis*. Amsterdam: Elsevier; 1985. vol. 24.
39. Deng Y, Flury M, Harsh JB, Felmy AR and Qafoku O. Cancrinite and sodalite formation in the presence of cesium, potassium, magnesium, calcium and strontium in Hanford tank waste stimulants. *Applied Geochemistry*. 2006; 21:2049-2063. <http://dx.doi.org/10.1016/j.apgeochem.2006.06.019>
40. Buhl JC, Stief F, Fechtelkord M, Gesing TM, Taphorn U and Taake C. Synthesis, X-ray diffraction and MAS NMR characteristics of nitrate cancrinite $\text{Na}_7[\text{AlSiO}_4]_6(\text{NO}_3)1.6(\text{H}_2\text{O})_2$. *Journal of Alloys and Compounds*. 2000; 305:93-102. [http://dx.doi.org/10.1016/S0925-8388\(00\)00724-6](http://dx.doi.org/10.1016/S0925-8388(00)00724-6)
41. Aronne A, Esposito S and Pernice P. FT-IR and DTA study of lanthanum aluminosilicates glasses. *Materials Chemistry and Physics*. 1997; 51:163-168. [http://dx.doi.org/10.1016/S0254-0584\(97\)80287-8](http://dx.doi.org/10.1016/S0254-0584(97)80287-8)
42. Aronne A, Esposito S, Ferone C, Pansini M and Pernice P. FT-IR study of the thermal transformation of barium-exchanged zeolite A to celsian. *Journal of Materials Chemistry*. 2002; 12:3039-3045. <http://dx.doi.org/10.1039/b203859e>
43. Wilson MA. *NMR Techniques and Applications in Geochemistry and Soil Chemistry*. Oxford: Pergamon Press; 1987.
44. Buhl JC and Löns J. Synthesis and crystal structure of nitrate enclathrated sodalite $\text{Na}_4[\text{AlSiO}_4]_6(\text{NO}_3)_2$. *Journal of Alloys and Compounds*. 1996; 235:41-47. [http://dx.doi.org/10.1016/0925-8388\(95\)02148-5](http://dx.doi.org/10.1016/0925-8388(95)02148-5)

45. Mundus C, Mueller-Warmuth W and Buhl JC. Crystallisation of a basic sodalite under hydrothermal conditions studied by MAS-NMR, XRD and DTA/DTG. *EJM European Journal of Mineralogy*. 1996; 8:231-239.
46. Covarrubias C, Garcia R, Arriagada R, Yanez J and Garland T. Cr(III) exchange on zeolites obtained from kaolin and natural mordenite. *Microporous and Mesoporous Materials*. 2006; 88:220-231. <http://dx.doi.org/10.1016/j.micromeso.2005.09.007>
47. Ocanto F, Acosta N, Linares CF and Urbina de Navarro C. Estudio de la influencia del par anionico $\text{NO}_3^-/\text{Br}^-$ en la sintesis del sistema cancrinita-sodialita. *Revista Latinoamericana de Metallurgia y Materiales*. 2007; 27:106-113.
48. Walton RI, Milange F, O'Hare D, Davies AT, Sankar G and Catlow CRA. An in situ energy dispersive X-ray diffraction study of the hydrothermal crystallization of zeolite A. 1. Influence of reaction condions and transformation into sodalite. *Journal of Physical Chemistry B*. 2001; 105:83-90. <http://dx.doi.org/10.1021/jp002711p>
49. Szostak R. *Molecular sieves*. London: Blackie Academic and Professional; 1998.
50. Ogura M, Kawazu T, Takahashi H and Okubo T. Aluminosilicate species in the hydrogel phase formed during the aging process for the crystallization of FAU zeolite. *Chemistry of Materials*. 2003; 15:2661-2667. <http://dx.doi.org/10.1021/cm0218209>
51. Lee S-R, Han Y-S, Park M, Park G-S and Choy J-H. Nanocrystalline Sodalite from Al_2O_3 Pillared Clay by Solid-Solid Transformation. *Chemistry of Materials*. 2003; 15:4841-4845. <http://dx.doi.org/10.1021/cm034614p>
52. Fechtelkord M, Posnatzki B and Buhl JC. Synthesis of basic cancrinite in a butanediol-water system. *Chemistry of Materials*. 2001; 13:1967-1975. <http://dx.doi.org/10.1021/cm001136z>